

STUDIES ON SHAPE MEMORY-COUPLED- PIEZOELECTRIC NANOCOMPOSITES

ANUPAM CHOWDHURY



**DEPARTMENT OF TEXTILE AND FIBRE ENGINEERING
INDIAN INSTITUTE OF TECHNOLOGY DELHI
JULY 2025**

© Indian Institute of Technology Delhi (IITD), New Delhi, 2025

**STUDIES ON SHAPE MEMORY-COUPLED-
PIEZOELECTRIC NANOCOMPOSITES**

by

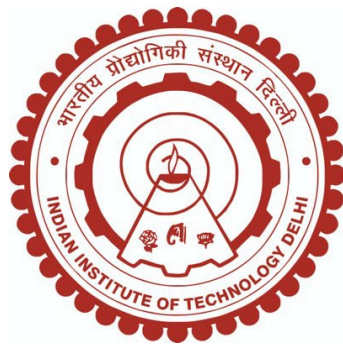
ANUPAM CHOWDHURY

Department of Textile and Fibre Engineering

Submitted

**in fulfilment of the requirements of the degree of
Doctor of Philosophy**

to the



Indian Institute of Technology Delhi

July 2025



Supreme Almighty

My grandfather (Late Santosh Kumar Sengupta)

Late Revered Swami Sagarananda ji Maharaj

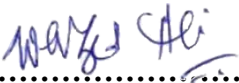
My loving parents Smt. Silpi Chowdhury and

Late Goutam Chowdhury

Certificate

This is to certify that the thesis entitled “**Studies on shape memory-coupled-piezoelectric nanocomposites**” being submitted by **Mr. Anupam Chowdhury**, to the Indian Institute of Technology Delhi, for the award of the degree of **Doctor of Philosophy** in the Department of Textile and Fibre Engineering, is a record of bonafide research work carried out by him. Mr. Chowdhury has worked under our guidance and supervision and fulfilled all the requirements for the submission of the thesis.

The results contained in this thesis have not been submitted, in part or full, to any other University or Institute for the award of any degree or diploma.



.....
Dr. S. Wazed Ali

Professor

Department of Textile and Fibre Engineering

Indian Institute of Technology Delhi

Hauz Khas

New Delhi 110016



.....
Dr. Bipin Kumar

Associate Professor

Department of Textile and Fibre Engineering

Indian Institute of Technology Delhi

Hauz Khas

New Delhi 110016

Acknowledgements

I would like to extend my heartiest gratitude to my Ph.D. Advisors, Dr. S Wazed Ali and Dr. Bipin Kumar for their unparalleled support and encouragement throughout the PhD journey. I would like to mention Wazed Sir's unconditional support with the resources of the laboratory to accomplish the research amidst several challenges, believed and supported me till the last mile. I also take this opportunity to mention Bipin Sir's support and encouragement which kept me going through thick and thin.

The journey to Ph.D. would not have been possible without the presence of my mother, Smt. Silpi Chowdhury, without whom I would not have traversed so long to this juncture of a long educational journey from kindergarten to doctoral degree. The early years of my life was marked by several memorable imprints of my father, Late Goutam Chowdhury who taught me Mathematics, Science and helped me to have a different insight towards the school curricula. Apart from my parents, my grandfather, Late Santosh Sengupta (Retired Railway Officer), was pivotal in mentoring me with different lessons of life and shaping me up for different educational milestones. I can still clearly remember the efforts put in by him to introduce me to different levels of Mathematics and English through different books purchased from College Street of erstwhile Calcutta. At this juncture, I take this opportunity to thank all my teachers at Happy Child High School (Raju Miss, Virginia Miss, Devjani Miss, Banani Miss, Ashok Sir, Kavita Miss) from kindergarten to 10th standard, who were very strict and took intense efforts for my overall growth and success. I also thank my English teacher Indrani Miss, Pritam Sir and Mathematics teacher Shankar Sir for supporting me till the last mile. Although I faced different financial challenges from time to time, but the divine energy always inspired me to try again and again till I succeeded in my goal.

The next major educational milestone which was truly a memorable one was marked by pursuing M.Tech in Polymer Science and Technology at Tezpur University. It was an enriching experience of two years, which helped me grow professionally and infused knowledge for the days to come. I would like to extend my deepest gratitude to Late. Prof. Mihir Kanti Chaudhari, Vice Chancellor of Tezpur University for granting me a semester fee waiver and being highly considerate to me during my crisis hours. I thank all my Professors at Department of Chemical Sciences, Prof. Niranjana Karak, Prof. Tarun K Maji and Prof Swapan K Dolui for introducing me the world of polymer science and technology and imbibing all the traits which was missed

in B.Tech studies. Needless to mention the immense support I received from my M. Tech thesis guide, Prof Swapan K Dolui during the thesis days and he is the only one, who still motivates me in this hard and strenuous PhD journey till date and believed in my abilities. Dr. Chandrama Sarkar, Dr. Jayashree Nath, Dr. Kankana Baruah, Dr. Priyankamoni Saikia, Dr. Kiranjyoti Mohan and all my M.Tech lab seniors will always hold a special place in my heart for providing me the perfect environment for research and continuous support. I also thank Dr. Nipu Dutta of Department of Chemical Sciences for introducing to the University staff families, who helped me by allowing me to teach their children, and this helped me to sustain myself during M.Tech. During that period, I am also elated to mention the efforts of Prof. Bibhash Chandra Das Purkayastha, ex-principal of Pandu College, Guwahati along with Ramakrishna Mission and Bharat Sevashram Sangha for supporting me with semester fees so that I could complete my M.Tech. These small and priceless efforts led to my journey to IIT Delhi.

The journey at IIT Delhi has been full of ups and downs, often marred by health issues. During my initial years of Ph.D., the reminiscences of interactions with Dr. Bapan Adak and Dr. Santanu Basak have always inspired me to work hard and keep on trying till I succeeded. I had the opportunity to learn lot of things from Bapan da, utilising by which I could accomplish my research goals. I would also like to thank Mr. Amarjit Singh, Mr. Khattar, Mr. Rohit Chikara from Fibre Science Laboratory and Dr. Veerender Sharma from Textile Chemistry Laboratory for helping me with their utmost capabilities from time to time. I was inspired to work much harder, when I bounced back after being attacked by deadly Dengue post Covid 2020 outbreak. Wazed Sir along with entire IIT Delhi fraternity stood tall and never stepped back in their efforts to recover me from my illness and giving me a new life. Needless to mention the tiring efforts of Mr. Sourav Banerjee who coordinated everything beside his Ph.D. studies, Mr. Amit Mandal, Mr. Gulshitab Aalam, and Dr. Jayashree Mohanty for being always by my side when I needed them the most. I also thank everyone, although I have missed them mentioning, their compassion and love made a lasting difference, and I remain truly grateful which helped me to bounce back from sick-bed with renewed vigour. I duly acknowledge all the colleagues of my laboratory and members of Fibre Science/Textile Chemistry laboratory for their support and special mentions for my junior friends, Dr. Subhadeep Paul and Mr. Srijan Das (now a Ph.D. student at NC State University), with whom my I could really resonate myself and had an opportunity to learn lot of things, collaborate and mentor. I sincerely thank Ms. Mandira Mondal and Ms. Mayuri Srivastava for always being just a call away for their unwavering support throughout my research journey. My gratitude to Mr. Rishabh Tiwari, Ms. Bharti Rana,

Ms. Suchita Tomar, Dr. Viraj Somkuwar, Dr. Hema Garg, Mr. Kumar Ghosh, Dr. Satyaranjan Bairagi, Mr. Sujaan Kaushik for their support all throughout. I would also like to thank Sourav's mother Mrs. Saraswati Banerjee for her affection and love. I also extend my love to my best friends, four-legged cat friend Miss. Tultuli and my pet cat Mr. Kulkul, who has been an important part of my Ph.D. journey as my extended family. I would also like to thank Dr Jaswant Hirwani for allowing me to use his lab facilities and sharing his different research insights. I owe my deepest gratitude to Prof Ratnamala Chatterjee and my friends Dr. Hitesh Gulati and Mr. Balwant Singh Chauhan for helping me with ferroelectric characterization, Dr. Subhankar Pandit and Dr. Dhrubajyoti Talukdar from IIT Guwahati, Ms. Shweta Nair and Mr. Vijay Mistari from IIT Bombay, Mr. Prakash Kurmi from Tezpur University and XRD characterization facilities of Saptarshi, IIT Jammu. I am also thankful to Mr. Supankar Das, for his help with new instruments, sharing enriching research talks for piezoelectric testing and Mr. Manoj Sinha from Keysight India for his all-round support with electrical characterization instruments. Without their help, I could not have accomplished my research objectives and travelled so far till date. I am also thankful to Mr. P Mazumder, Mrs. S Mazumder and Dr. P Mazumder for always motivating and supporting me whenever I felt low. I am highly indebted to Prof. Mangala Joshi for allowing me to use her research and fabrication facilities, motivated and helped me with the best of her abilities. I am also thankful to everyone from Central Research Facility (special mentions for Ms. Aastha Sharma, Mr. Mahesh Soni, Mr. Kuldeep Sharma, Dr. Atul Kr Singh, Dr. Somendra Singh, Mr. Dinesh Kumar, Mr. Shivprakash Solanki, Mr. Rajesh Kumar, Mr. Pradeep Kumar, Mr. Manoj Kumar Jaiswal, Dr Samim Hassan) and Nanoscale Research Facility. I am also thankful to my house owners Col. Rajesh Sharma and Mrs Nirmal Garg for allowing me to stay at their place which helped me to devote my time towards studies without any hassle. Last but not the least, I am thankful to my SRC committee members, Prof Mangala Joshi, Prof. Rajiv K Srivastava and Dr. Puspapraj Singh for being supportive and providing me valuable feedback for my research studies from time to time. I am thankful to my thesis examiners, Prof. Prasanth Raghavan and Prof. Henry Wi, Li for their valuable feedback for the thesis. Once again, I extend my heartfelt gratitude to my mother for her unwavering support throughout this long and enriching Ph.D. journey and never lost faith in my abilities. I am also deeply indebted to the blessings of my father and grandfather, who have always been with me like stars twinkling brightly located light years away.

Anupam Chowdhury

Anupam Chowdhury

Abstract

The recent times have witnessed an upsurge in growth of smart materials that can perform multiple functions within a single system. These materials can sense and respond to their environment, thereby making them indispensable for next generation technologies. There is a rising demand to probe further into the design of these materials particularly meant for sensing and actuation. Among many types of smart materials like electroactive polymers, magnetostrictive materials, self-healing systems, there are two interesting categories, i.e., combination of shape memory and piezoelectric materials which may be very useful for sensing and actuation. Their ability to respond to external stimuli surpasses them for exciting future applications.

The thesis deals with development of shape memory-coupled-piezoelectric nanocomposites, which was accomplished by (i) combining shape memory and piezoelectric polymer and (ii) combining shape memory polymer and piezoelectric filler. Therefore, by these two approaches, we can clearly distinguish the synergism between polymer-polymer and polymer-filler system. Initially, blends of polyurethane and PVDF was processed by melt extrusion to prepare filaments possessing higher relative piezoelectric β phase of 66 %. The alignment of polymer chains along the fibre axis during melt extrusion resulted in the transformation of α to β transformation of PVDF without additional stretching and poling. The open-circuit voltage and short-circuit current was 280 mV and 0.154 μ A, respectively for the blends. The addition of optimum r-GO promoted α phase and increased conductivity leading to an open circuit voltage of 349 mV and short-circuit current of 0.257 μ A. The strain recovery value of 100% and fixity of 43% was observed at 50/50 PU-PVDF blends, whereas recovery of 100% and fixity of 46% was observed for PU/PVDF-0.3% rGO nanocomposite blends. The crystallinity and morphology of piezoelectric fillers plays an important role in tuning electromechanical and piezoelectric properties of the nanocomposites. Therefore, ZnSnO_3 (ZT) was chosen as the self-polled piezoelectric filler whose crystallinity was tuned primarily through varying concentration of NaOH and morphology was controlled through concentration of capping agent along with physical and chemical parameters. Lower mineralizer concentration promoted different polycrystalline species like SnO_2 and Zn_2SnO_4 exhibiting nanoparticle morphologies. Higher mineralizer concentration promoted the formation of face centred cubic zinc hydroxystannate phase, exhibiting ideal ferroelectric behaviour and promising piezoelectric behaviour. Further, tuning ($(\text{Zn}^{2+}$ or $\text{Sn}^{4+})$ / urea) (m) promoted formation of high aspect ratio nanorods having aspect ratio of $\sim 7.95 \pm 2.55$ at a fixed mineralizer concentration, fill volume, temperature and

time of the reaction. The thorough and systematic study was conducted to study the effect of physical and chemical parameters to obtain one step ZT nanorods. The nanorods synthesized at different m ratios were tested for ferroelectric, dielectric and piezoelectric properties. The high aspect nanorods had remnant polarization of $0.11 \mu\text{C}/\text{cm}^2$, lossy ferroelectric behaviour and showed effective piezoelectric coefficient of $0.20 \text{ pm}/\text{V}$.

In the next part of the research, the ZT nanocubes synthesized using 0.25 M mineralizer and high aspect nanorods synthesized using $m=0.04$ were used as the piezoelectric filler in SMPU matrix for the preparation of nanocomposites in the form of solvent cast films, melt spun fibres and electrospun nanofibres. The solvent cast nanocomposite films were prepared by using ZT nanocubes. The highest dielectric constant of 5.039 was shown by SMPU-5%ZT among all samples. PZ-5 displayed strain fixity of 88.89% and strain recovery of 87.5% at the end of 1st cycle due to the presence of filler, which further enhanced to 100% at the end of 2nd and 3rd cycle. PZ-5 shown highest peak-to-peak open-circuit voltage of 3.26 V , short-circuit current of $1.13 \mu\text{A}$, charge measured in shielded and unshielded mode was 0.26 nC and 2.2 nC , and power density of $\sim 2.12 \text{ mW}/\text{m}^2$ at $8.2 \text{ M}\Omega$. The output of nanogenerator was used for charging a capacitor and lighting up an LED. The shape customized PZ-5 displayed potential applications as touch sensor and temperature sensors. The melt spun SMPU/ZT nanocomposite filaments were fabricated by employing ZT nanorods. It displayed open-circuit voltage and short-circuit current of $\sim 3.69 \text{ V}$ and $\sim 0.52 \mu\text{A}$, power density of $1.16 \text{ mW}/\text{m}^2$ at load resistance of $10 \text{ M}\Omega$. The generated voltage was used to power LED, thereby indicating its practical real-life implementations. The shape memory behaviour of PZ-0.75 showed 100% strain fixity and strain recovery at the end of 3rd cycle of repeated training of loading and unloading cycles. The multifunctional woven fabric made of PZ-0.75 was used to monitor wrist movements. The structure-property relationship of ZT nanocubes and nanorods was studied in electrospinning process. The interesting thermal transitions were observed for addition of fillers in SMPU matrix. The highest piezoelectric output was observed at 1% concentration of nanorods (peak-to-peak open-circuit voltage of $\sim 2.20 \text{ V}$, short-circuit current of $\sim 1.31 \mu\text{A}$, power density of $2.6 \text{ mW}/\text{m}^2$ at $1 \text{ M}\Omega$ load resistance) and nanocubes (peak-to-peak open-circuit voltage of $\sim 1.4 \text{ V}$, short-circuit current of $\sim 1.25 \mu\text{A}$, power density of $\sim 1.2 \text{ mW}/\text{m}^2$ at $680 \text{ k}\Omega$) in SMPU nanofibres. It showed promising real-life applications as multifunctional material responding to different flex movements of a finger and tracking repeated respiratory movements. It showed promising shape memory behaviour. Therefore, the developed multifunctional nanocomposites are promising in the field of sensors, actuators and energy harvesters.

सार

हाल के समय में ऐसे स्मार्ट पदार्थों के विकास में तेज़ी देखी गई है जो एक ही प्रणाली में कई कार्य कर सकते हैं। ये पदार्थ अपने परिवेश को महसूस कर सकते हैं और उस पर प्रतिक्रिया दे सकते हैं, जिससे ये अगली पीढ़ी की तकनीकों के लिए अपरिहार्य हो जाते हैं। इन पदार्थों के डिज़ाइन, विशेष रूप से संवेदन और क्रियान्वयन के लिए, और अधिक गहन अध्ययन की माँग बढ़ रही है। इलेक्ट्रोएक्टिव पॉलिमर, मैग्नेटोस्ट्रिक्टिव पदार्थ, स्व-उपचार प्रणालियाँ जैसे कई प्रकार के स्मार्ट पदार्थों में, दो दिलचस्प श्रेणियाँ हैं, अर्थात् आकार स्मृति और पीज़ोइलेक्ट्रिक पदार्थों का संयोजन, जो संवेदन और क्रियान्वयन के लिए बहुत उपयोगी हो सकते हैं। बाहरी उत्तेजनाओं पर प्रतिक्रिया करने की उनकी क्षमता भविष्य के रोमांचक अनुप्रयोगों के लिए उनसे कहीं बेहतर है।

यह शोध प्रबंध आकार स्मृति-युग्मित-पीज़ोइलेक्ट्रिक नैनोकंपोजिट के विकास से संबंधित है, जिसे (i) आकार स्मृति और पीज़ोइलेक्ट्रिक पॉलीमर के संयोजन और (ii) आकार स्मृति पॉलीमर और पीज़ोइलेक्ट्रिक फिलर के संयोजन द्वारा पूरा किया गया था। इसलिए, इन दो तरीकों से, हम पॉलीमर-पॉलिमर और पॉलीमर-फिलर प्रणाली के बीच तालमेल को स्पष्ट रूप से पहचान सकते हैं। प्रारंभ में, पॉलीयुरेथेन और PVDF के मिश्रणों को 66% के उच्च सापेक्ष पीज़ोइलेक्ट्रिक β चरण वाले फिलामेंट तैयार करने के लिए मेल्ट एक्सट्रूज़न द्वारा संसाधित किया गया था। मेल्ट एक्सट्रूज़न के दौरान फाइबर अक्ष के साथ पॉलीमर श्रृंखलाओं के संरेखण के परिणामस्वरूप अतिरिक्त स्ट्रेचिंग और पोलिंग के बिना PVDF का α से β रूपांतरण हुआ। इष्टतम r-GO के संयोजन से α चरण में वृद्धि हुई और चालकता में वृद्धि हुई, जिससे 349 mV का खुला परिपथ वोल्टेज और 0.257 μ A का लघु-परिपथ धारा प्राप्त हुई। 50/50 PU-PVDF मिश्रणों में 100% विकृति पुनर्प्राप्ति मान और 43% स्थिरता देखी गई, जबकि PU/PVDF-0.3% rGO नैनोकंपोजिट मिश्रणों में 100% पुनर्प्राप्ति और 46% स्थिरता देखी गई। नैनोकंपोजिट के विद्युत-यांत्रिक और

पीजोइलेक्ट्रिक गुणों को समायोजित करने में पीजोइलेक्ट्रिक भरावों की क्रिस्टलीयता और आकारिकी महत्वपूर्ण भूमिका निभाती है। इसलिए, $ZnSnO_3$ (ZT) को स्व-ध्रुवित पीजोइलेक्ट्रिक भराव के रूप में चुना गया, जिसकी क्रिस्टलीयता को मुख्य रूप से NaOH की बदलती सांद्रता के माध्यम से समायोजित किया गया और आकारिकी को भौतिक और रासायनिक मापदंडों के साथ कैपिंग एजेंट की सांद्रता के माध्यम से नियंत्रित किया गया। कम खनिज सांद्रता ने नैनोकणों की आकारिकी प्रदर्शित करने वाले SnO_2 और Zn_2SnO_4 जैसी विभिन्न पॉलीक्रिस्टलाइन प्रजातियों को बढ़ावा दिया। उच्च खनिज सांद्रता ने फलक केंद्रित क्यूबिक जिंक हाइड्रॉक्सीस्टैनेट चरण के निर्माण को बढ़ावा दिया, जिसने आदर्श फेरोइलेक्ट्रिक व्यवहार और आशाजनक पीजोइलेक्ट्रिक व्यवहार प्रदर्शित किया। एक-चरण ZT नैनोरॉड प्राप्त करने के लिए भौतिक और रासायनिक मापदंडों के प्रभाव का अध्ययन करने हेतु एक गहन और व्यवस्थित अध्ययन किया गया। विभिन्न $Zn^{2+}/urea$ अनुपातों पर संश्लेषित नैनोरॉड्स का फेरोइलेक्ट्रिक, डाइइलेक्ट्रिक और पीजोइलेक्ट्रिक गुणों के लिए परीक्षण किया गया। उच्च अभिमुखता वाले नैनोरॉड्स में $0.11 \mu C/cm^2$ का अवशिष्ट ध्रुवीकरण, हानिपूर्ण फेरोइलेक्ट्रिक व्यवहार और 0.20 pm/V का प्रभावी पीजोइलेक्ट्रिक गुणांक प्रदर्शित हुआ। शोध के अगले भाग में, 0.25 M मिनीरलाइज़र का उपयोग करके संश्लेषित ZT नैनोक्यूब्स और $m=0.04$ का उपयोग करके संश्लेषित उच्च आस्पेक्ट नैनोरॉड्स का उपयोग SMPU मैट्रिक्स में पीजोइलेक्ट्रिक फिलर के रूप में किया गया ताकि सॉल्वेंट कास्ट फ़िल्म्स, मेल्ट स्पिन फ़ाइबर और इलेक्ट्रोस्पिन नैनोफ़ाइबर के रूप में नैनोकंपोज़िट तैयार किए जा सकें। सॉल्वेंट कास्ट नैनोकंपोज़िट फ़िल्में ZT नैनोक्यूब्स का उपयोग करके तैयार की गईं। सभी नमूनों में SMPU-5%ZT ने 5.039 का उच्चतम परावैद्युत स्थिरांक दर्शाया। PZ-5 ने फिलर की उपस्थिति के कारण पहले चक्र के अंत में 88.89% की विकृति स्थिरता और 87.5% की विकृति पुनर्प्राप्ति प्रदर्शित की, जो दूसरे और तीसरे चक्र के अंत में 100% तक बढ़ गई। PZ-5 ने 3.26 V का उच्चतम पीक-टू-पीक ओपन-सर्किट वोल्टेज, $1.13 \mu A$ का शॉर्ट-सर्किट करंट, परिरक्षित और अप्रतिरक्षित मोड में मापा गया चार्ज 0.26 nC और 2.2 nC , और $8.2 \text{ M}\Omega$

पर $\sim 2.12 \text{ mW/m}^2$ का पावर घनत्व दिखाया। नैनोजनरेटर के आउटपुट का उपयोग एक संधारित्र को चार्ज करने और एक LED को प्रकाशित करने के लिए किया गया था। आकार अनुकूलित PZ-5 ने टच सेंसर और तापमान सेंसर के रूप में संभावित अनुप्रयोगों को प्रदर्शित किया। पिछले हुए SMPU/ZT नैनोकंपोजिट फिलामेंट्स को ZT नैनोरॉड्स का उपयोग करके तैयार किया गया था। इसने $10 \text{ M}\Omega$ के लोड प्रतिरोध पर 1.16 mW/m^2 का ओपन-सर्किट वोल्टेज और शॉर्ट-सर्किट करंट $\sim 3.69 \text{ V}$ और $\sim 0.52 \mu\text{A}$, पावर घनत्व 1.16 mW/m^2 प्रदर्शित किया। उत्पन्न वोल्टेज का उपयोग एलईडी को पावर देने के लिए किया गया था, जिससे इसके व्यावहारिक वास्तविक जीवन के कार्यान्वयन का संकेत मिलता है। PZ-0.75 के आकार स्मृति व्यवहार ने लोडिंग और अनलोडिंग चक्रों के दोहराया प्रशिक्षण के तीसरे चक्र के अंत में 100% तनाव स्थिरता और तनाव वसूली दिखाई। कलाई की गतिविधियों पर नज़र रखने के लिए PZ-0.75 से बने बहुक्रियाशील बुने हुए कपड़े का उपयोग किया गया था एसएमपीयू नैनोफाइबर में नैनोरॉड्स ($\sim 2.20 \text{ V}$ का पीक-टू-पीक ओपन-सर्किट वोल्टेज, $\sim 1.31 \mu\text{A}$ का शॉर्ट-सर्किट करंट, $1 \text{ M}\Omega$ लोड प्रतिरोध पर 2.6 mW/m^2 का पावर घनत्व) और नैनोक्यूब्स ($\sim 1.4 \text{ V}$ का पीक-टू-पीक ओपन-सर्किट वोल्टेज, $\sim 1.25 \mu\text{A}$ का शॉर्ट-सर्किट करंट, $680 \text{ k}\Omega$ पर $\sim 1.2 \text{ mW/m}^2$ का पावर घनत्व) की 1% सांद्रता पर उच्चतम पीजोइलेक्ट्रिक आउटपुट देखा गया। इसने एक उंगली के विभिन्न फ्लेक्स मूवमेंट पर प्रतिक्रिया करने और बार-बार होने वाली श्वसन गतिविधियों को ट्रैक करने वाले बहुक्रियाशील पदार्थ के रूप में आशाजनक वास्तविक जीवन के अनुप्रयोगों को दिखाया। इसने आशाजनक आकार स्मृति व्यवहार दिखाया। इसलिए, विकसित बहुक्रियाशील नैनोकंपोजिट सेंसर, एक्चुएटर्स और ऊर्जा संग्राहकों के क्षेत्र में आशाजनक हैं।

Table of Contents

Certificate	i
Acknowledgements.....	ii
Abstract	v
LIST OF ABBREVIATIONS	xxi
1 Chapter 1 Introduction and Objectives	1
1.1 General Background.....	1
1.2 Motivation.....	3
1.3 Objectives.....	3
1.4 Outline of the thesis	4
1.5 Organization of the thesis.....	5
2 Chapter 2 Literature review.....	9
2.1 Theory of piezoelectricity	9
2.1.1 Lead based piezoelectric ceramics.....	12
2.1.2 Lead-free piezoelectric ceramics	14
2.1.3 Piezoelectric polymers	16
2.1.4 Piezoelectric nanocomposites.....	18
2.2 Shape memory materials.....	19
2.2.1 Shape memory nanocomposites	21
2.3 Shape memory- assisted piezoelectric materials	22
2.3.1 Combined shape memory and piezoelectric effect in shape memory alloys.	23
2.3.2 Combined shape memory and piezoelectric effect in shape memory polymers	25
2.4 Critical Analysis and Identification of Research Gaps.....	28
2.5 Summary.....	29
3 Chapter 3 Development of shape memory-coupled-piezoelectric material using PVDF/PU blend and its structure property analysis.....	31

3.1	Introduction	31
3.2	Materials and Methods	32
3.2.1	Preparation of composite filaments	32
3.2.2	Characterizations	33
3.3	Results and Discussion	36
3.3.1.1	Functional group analysis by ATR-FTIR	36
3.3.1.2	Thermal characterization by Differential Scanning Calorimetry (DSC)	38
3.3.1.3	Crystallinity determination by X-ray diffraction analysis (XRD)	39
3.3.2	Evaluation of energy harvesting efficiency by digital oscilloscope	42
3.4	Evaluation of shape memory properties of the nanocomposite filaments	49
3.5	Analysis of tensile properties of the nanocomposite filaments	51
3.6	Surface morphology analysis by FESEM	53
4	Chapter 4 Synthesis of Zinc tin oxide and its process parameter optimization to investigate its structural influence on ferroelectric properties to obtain optimum piezoelectric effect	55
4.1	Effect of mineralizer NaOH on ferroelectric and piezoelectric properties of Zinc tin oxide	55
4.1.1	Introduction	55
4.1.2	Synthesis of Zinc stannate nanostructures	57
4.1.2.1	Measurement of ferroelectric and dielectric properties	57
4.1.2.2	Measurement of piezoelectric properties	58
4.1.2.3	Structural and morphological characterization	58
4.1.3	Results and Discussion	59
4.1.3.1	Crystalline transition study by XRD	59
4.1.3.2	Raman spectroscopy study of different phonon modes in crystalline transitions	61
4.1.3.3	Morphological transition study by SEM and TEM	62
4.1.3.4	Band gap transition study by UV-vis spectroscopy	66

4.1.3.5	Thermal transition study of different crystalline phases by TGA.....	67
4.1.3.6	Analysis of dielectric behaviour of ZS samples synthesized at different mineralizer concentration by LCR	68
4.1.3.7	Analysis of ferroelectric properties of ZS samples synthesized at different mineralizer concentration by P-E loop tracer	71
4.1.3.8	Analysis of piezoelectric properties by PFM.....	72
4.1.4	Summary.....	73
4.2	Tuning the rod like morphology of Zinc tin oxide by Zn^{2+} /Urea ratio.....	75
4.2.1	Introduction.....	75
4.2.2	Materials and Methods.....	77
4.2.2.1	Synthesis of $ZnSnO_3$ (ZT) nanorods	77
4.2.2.2	Structural and morphological characterization.....	78
4.2.2.3	Measurement of ferroelectric and dielectric properties	78
4.2.2.4	Measurement of piezoelectric properties	78
4.2.3	Results and Discussion.....	79
4.2.3.1	Effect of Zn^{2+} /urea ratio on the growth of nanostructures.....	79
4.2.3.2	Effect of mineralizer on the growth of nanorods	84
4.2.3.3	Effect of hydrothermal synthesis temperature on the growth of nanorods..	86
4.2.3.4	Effect of time on the growth of nanorods	88
4.2.3.5	Growth mechanism of $ZnSnO_3$ nanorods.....	88
4.2.3.6	Effect of Zn^{2+} /urea ratio on dielectric and ferroelectric properties	89
4.2.3.7	Effect of Zn^{2+} /urea ratio on piezoelectric properties	91
4.2.4	Summary.....	92
5	Study on the effect of Zinc tin oxide on piezoelectric and shape memory properties of PU based solvent cast nanocomposite film.....	93
5.1	Introduction.....	93
5.2	Materials and Methods.....	95
5.2.1	Preparation of nanocomposite films.....	95

5.2.2	Characterization of nanocomposite film.....	95
5.2.2.1	Structural and morphological characterization.....	95
5.2.2.2	Measurement of ferroelectric, dielectric, piezoelectric and shape memory properties.....	96
5.2.2.3	Fabrication of piezoelectric device and testing procedure.....	96
5.3	Results and Discussion.....	98
5.3.1	Structural, functional group, thermal transition and morphology analysis	98
5.3.2	Analysis of ferroelectric and dielectric properties	102
5.3.3	Analysis of shape memory properties	104
5.3.4	Analysis of piezoelectric properties	105
5.4	Utility of PZ-5 for multifaceted applications.....	110
5.4.1	Shape conformable PZ-5 as a touch sensor	110
5.4.2	Shape conformable PZ-5 as a temperature sensor	111
5.5	Summary.....	113
6	Study on the effect of Zinc tin oxide nanorods on piezoelectric and shape memory properties of PU based melt extruded filament.....	114
6.1	Introduction.....	114
6.2	Materials and Methods.....	116
6.2.1	Preparation of SMPU melt-spun filament.....	116
6.2.2	Morphology, Structural and Thermal characterization.....	117
6.2.3	Measurement of piezoelectric and shape memory properties	117
6.3	Results and Discussion.....	118
6.3.1	Morphological characterization using FESEM, functional group interactions by FTIR and crystallinity determination by XRD	118
6.3.2	Thermal transition study by DSC	123
6.3.3	Analysis of piezoelectric properties	124
6.3.4	Analysis of shape memory properties by thermomechanical characterization and piezoelectric properties by PFM	126

6.4	Application as multifunctional sensors	128
6.5	Summary.....	130
7	Study on the effect of Zinc tin oxide of different morphology (nanorods and nanocubes) on piezoelectric and shape memory properties of PU based electrospun nanofibre	131
7.1	Introduction.....	131
7.2	Materials and Methods.....	133
7.2.1	Preparation of SMPU electrospun nanocomposites	133
7.2.2	Morphology, Structural and Thermal characterization.....	133
7.2.3	Measurement of piezoelectric and shape memory behaviour.....	134
7.3	Results and Discussion.....	136
7.3.1	Morphological, structural and thermal analysis.....	136
7.3.2	Analysis of piezoelectric and shape memory properties	143
7.4	Utility as multifunctional sensors	152
7.4.1	Use as a conformable sensor to detect flex movements of a finger.....	152
7.4.2	Use as a piezoelectric sensor for monitoring respiratory movements.....	154
7.5	Summary.....	155
8	Chapter 8 Summary and future scope of the work.....	157
8.1	Summary of the research work.....	157
8.2	Conclusions.....	157
8.3	Limitations of the present study	162
8.4	Future scope	163
	APPENDIX.....	164
	References.....	171

List of Figures

Figure 2.1 Representation of coupling between different physical systems (b) Representative stress-strain behaviour of an elastic material ⁸	10
Figure 2.2 (a) Direct piezoelectric effect (b) relationship between electrical displacement and stress in a piezoelectric material ⁸	11
Figure 2.3 Piezoelectric constants of lead based and lead-free piezoelectric ceramics. ¹⁵	13
Figure 2.4 Research documents (article, proceeding paper, review article, early access, correction, editorial matter, meeting abstract and letters) having the keywords lead free AND piezoelectric AND ceramic in the span of 2001- 2025 as gathered from Clarivate Web of Science	14
Figure 2.5 ZnO ₆ and SnO ₆ forming an octahedron framework responsible for being self-poled as seen in ZnSnO ₃ ⁵	16
Figure 2.6 α , β , γ phases as seen in PVDF ⁴⁰	17
Figure 2.7 (a) Output voltage generated from 2 wt% MgO/P(VDF-TrFE) nanocomposite and d_{33} values as a function of different bending cycles ⁴⁸ (b) Device architecture and SEM morphology of PDMS/ZnSnO ₃ /CNT nanocomposite device ⁴⁹	19
Figure 2.8 Shape memory experiment depicting the shape/strain fixity and shape/strain recovery of the nanocomposite at temperatures greater than T _g or less than T _g , where T _g is the transition temperature based on T _g / T _m type shape memory polyurethane	21
Figure 2.9 (a) Schematic of robotic hand, ⁶⁴ (b) mosquito bite inspired pumping mechanism ⁶⁵	24
Figure 2.10 (a) Molecular networks in water responsive actuator and energy generator, ⁷¹ (b) 4D printed magnetolectric device and piezoelectric voltage output from the device ⁷²	26
Figure 3.1 Possible interactions between shape memory polyurethane (PU), polyvinylidene fluoride (PVDF) and r-GO	32
Figure 3.2 Shape memory experiment depicting the strain fixity and strain recovery of the composite filaments at programmed temperature of 60 °C.	35
Figure 3.3 ATR-FTIR spectra of the samples in the (a) region of 1750 cm ⁻¹ to 1500 cm ⁻¹ , and (b) 855 cm ⁻¹ to 600 cm ⁻¹	36
Figure 3.4 ATR-FTIR spectra of (a) composite filaments, and (b) r-GO	37
Figure 3.5 DSC scans showing (a) melting transitions in 1 st heating cycle, (b) shifted T _g and T _m of soft segment PCL 2000 in 50/50 blends of PVDF and PU, and (c) T _m of soft segment PCL 2000 in PU	38

Figure 3.6 DSC thermograms (exotherm up) depicting shift of T_g 's of soft segment PCL 2000 in the composite filaments (a) P5PV5-0.1R, (b) P5PV5-0.3R, and (c) P5PV5-0.5R.....	39
Figure 3.7 Deconvoluted curves of XRD patterns at 18.3 °, 19.9 ° and 20.8 ° of pristine (a) PVDF, (b) P5PV5-0R, (c) P5PV5-0.1R, (d) P5PV5-0.3R, and (e) P5PV5-0.5R showing the experimental data in dotted lines and solid lines representing the best fit.....	40
Figure 3.8 XRD plots of (a) composite filaments, and (b) in the region between 2θ (°) of 15 and 25.....	41
Figure 3.9 Open-circuit voltages of (a) PVDF, (b) P5PV5-0R, (c) P5PV5-0.3R, (d) actual device prototype, and (e) schematic of open-circuit voltage captured by oscilloscope.....	42
Figure 3.10 The energy harvesting mechanism of DUT (device under test) under the influence of compressive forces by tapping mechanism	43
Figure 3.11 Open-circuit voltages of (a) P5PV5-0.1R, and (b) P5PV5-0.5R.....	44
Figure 3.12 Voltage across load resistance of 8.2 M Ω of (a) PVDF, (b) P5V5-0R, (c) P5PV5-0.3R, and (d) Power density of the samples at load resistance of 8.2 M Ω	45
Figure 3.13 Short-circuit current plots of (a) PVDF, (b) P5PV5-0R, (c) P5PV5-0.3R and closed-circuit current plots under load resistance of 10 M Ω of (d) PVDF, (e) P5PV5-0R, (f) P5PV5-0.3R	46
Figure 3.14 Short-circuit currents of (a) P5PV5-0.1R, (b) P5PV5-0.5R, closed-circuit currents across load resistance of 10 M Ω of (c) P5PV5-0.1R, and (d) P5PV5-0.5R	47
Figure 3.15 Plot of data to find out internal resistance (a) PVDF, and (b) P5PV5-0.3R from voltage across load resistance values (1 to 10 M Ω)	47
Figure 3.16 Plot of data to find out internal resistance (a) P5PV5-0R, (b) P5PV5-0.1R, (c) P5PV5-0.5R	48
Figure 3.17 (a-e) Thermo-mechanical shape memory characterization of the filaments (PU, P5PV5-0R, P5PV5-0.1R, P5PV5-0.3R, P5PV5-0.5R) where (1), (2) and (3) are the number of cycles.	49
Figure 3.18 Strain fixity and recovery percentages of the various samples in third cycle of shape memory tests	50
Figure 3.19 (a). Average modulus values of (i) PVDF, (ii) PU, (iii) P5PV5-0R, (iv) P5PV5-0.1R, (v) P5PV5-0.3R, (vi) P5PV5-0.5R , and (b) Load vs Elongation values of the same samples.....	51
Figure 3.20 FESEM of (a). P5PV5-0R, (b). P5PV5-0.1R, (c). P5PV5-0.3R, (d). P5PV5-0.5R	53

Figure 4.1.1 XRD plots of synthesized samples at 0 M, 0.05 M NaOH concentration and ICDD reference patterns	59
Figure 4.1.2 XRD plots of synthesized samples at 0.15 M, 0.25 M NaOH concentration and ICDD reference patterns [Note: Miller indices are indexed as per ICDD 33-1376]	60
Figure 4.1.3 Raman spectra of ZS synthesized using 0 M - 0.25 M NaOH measured at room temperature using 514 nm laser	61
Figure 4.1.4 SEM images of (a) - (d) ZS synthesized with 0 - 0.25 M NaOH	62
Figure 4.1.5 TEM images of (a) - (d) ZS synthesized with 0 - 0.25 M NaOH	63
Figure 4.1.6 Size distribution plots of (a)-(d) ZS synthesized using 0 M – 0.25 M mineralizer NaOH as examined by SEM	64
Figure 4.1.7 Inverted colour image of (a)-(b) ZS synthesized using 0 M and 0.05 M NaOH, (c)-(d) single crystal diffraction spots in SAED pattern of ZS synthesized using 0.15 M and 0.25 M NaOH as examined by TEM	64
Figure 4.1.8 EDX analysis of ZS synthesized with (a) 0 M, (b) 0.05 M, (c) 0.15 M, (d) 0.25 M	65
Figure 4.1.9 FTIR spectra of ZS synthesized with (a) 0 M, (b) 0.05 M, (c) 0.15 M, (d) 0.25 M	65
Figure 4.1.10 UV-vis spectra and Tauc plots of ZS synthesized with (a) 0 M, (b) 0.05 M, (c) 0.15 M, (d) 0.25 M	66
Figure 4.1.11 TGA response with different mass loss transition and differential thermogravimetry of ZS synthesized with (a) 0 M, (b) 0.05 M, (c) 0.15 M, (d) 0.25 M	67
Figure 4.1.12 (a) - (b) Dielectric constant and (c) - (d) dissipation factor of ZS synthesized with 0 M, 0.05 M, 0.15 M, and 0.25 M	68
Figure 4.1.13 (a) Dielectric constant and (b) Dissipation factor of the ZS synthesized at different mineralizer NaOH concentrations	70
Figure 4.1.14 AC conductivity plots of ZS synthesized (a) without and 0.05 M mineralizer, (b) 0.15 M and 0.25 M mineralizer	70
Figure 4.1.15 Ferroelectric hysteresis loops of (a) - (d) ZS synthesised using 0 M – 0.25 M NaOH	71
Figure 4.1.16 Amplitude vs phase of ZS synthesised using (a) 0 M, (b) 0.05 M, (c) 0.15 M and (d) 0.25 M NaOH, as studied by PFM	72
Figure 4.1.17 DART-PFM images representing surface topography at 6 random scan points of ZS synthesized using (a) without mineralizer, (b) 0.05 M mineralizer, (c) 0.15 M mineralizer (d) 0.25 M mineralizer	72

Figure 4.2.1 XRD spectra of ZT nanostructures synthesized using $Zn^{2+}/urea = 0.02, 0.04, 0.06$, without urea and ICDD reference patterns for comparison	79
Figure 4.2.2 FESEM images of ZT synthesized using (a) $m = 0.02$, (b) $m = 0.04$, (c) $m = 0.06$ and HRTEM images of ZT synthesized using (d) $m = 0.02$, (e) $m = 0.04$, (f) $m = 0.06$	80
Figure 4.2.3 HRTEM images denoting lattice fringe of ZT synthesized using (a) $m = 0.02$, (b) $m = 0.04$, (c) $m = 0.06$	80
Figure 4.2.4 (a) FESEM image, (b) TEM image of ZT synthesized without urea	81
Figure 4.2.5 (a)-(d) TEM images of the ZT nanorods synthesized using $m = 0.04$ at different time periods	82
Figure 4.2.6 Raman spectra of ZT synthesized using (a) $m = 0.02$, (b) $m = 0.04$ and (c) $m = 0.06$	83
Figure 4.2.7 XRD spectra of ZT synthesized using (a) without mineralizer (0 M), (b) 0.09 M, (c) 0.11 M, (d) 0.13 M, (e) 0.15 M, (f) 0.20 M	84
Figure 4.2.8 FESEM images of ZT synthesized using (a) 0 M, (b) 0.09 M, (c) 0.13 M, (d) 0.15 M, (e) 0.20 M	85
Figure 4.2.9 TEM image of ZT synthesized without mineralizer and urea	86
Figure 4.2.10 XRD spectra of ZT samples synthesized at 180 °C, 220 °C and reference ICDD patterns	86
Figure 4.2.11 FESEM images of ZT samples synthesized at (a) 180 °C, (b) 220 °C and TEM images of ZT samples synthesized at (c) 180 °C, (d) 220 °C	87
Figure 4.2.12 FESEM images of ZT samples synthesized at (a) room temperature, (b) 6 h, (c) 12 h, (d) 18 h, (e) 26 h	88
Figure 4.2.13 Dielectric constant and $\tan \delta$ of ZT synthesized using (a) $m = 0.02$, (b) $m = 0.04$, (c) $m = 0.06$ and ferroelectric hysteresis plots of ZT synthesized using (d) $m = 0.02$, (e) $m = 0.04$, (f) $m = 0.06$	89
Figure 4.2.14 Amplitude vs phase of ZT synthesized using (a) $m = 0.02$, (b) $m = 0.04$ and (c) $m = 0.06$, derived from PFM spectroscopy	91
Figure 5.1 FESEM of (a) PZ-0, (b) PZ-2.5, (c) PZ-5, (d) PZ-10, (e) PZ-15	98
Figure 5.2 EDX OF PZ-2.5	98
Figure 5.3 (a) XRD patterns and (b) FTIR-ATR spectra of SMPU nanocomposites	99
Figure 5.4 FTIR of PZ-0 and PZ-5 in wavenumber region of (a) 4000-2500 cm^{-1} and (b) 1800-1600 cm^{-1}	100
Figure 5.5 DSC of (a) cooling cycle, (b) 2 nd heating cycle of SMPU based nanocomposites	101

Figure 5.6 Melting endotherms of (a) PZ-0, (b) PZ-2.5, (c) PZ-5, (d) PZ-10 and (e) PZ-15	101
Figure 5.7 P-E hysteresis loops of (a) PZ-0, (b) PZ-2.5, (c) PZ-5, (d) PZ-10, (e) PZ-15	102
Figure 5.8 (a) Dielectric constant and (b) dissipation factor of PZ-0, PZ-2.5, PZ-5, PZ-10 and PZ-15	103
Figure 5.9 (a) Shape memory cycle of PZ-2.5 and strain fixity % and recovery % of (b) PZ-0 and (c) PZ-5	104
Figure 5.10 Strain fixity % and recovery % of (a) PZ-2.5 and (b) PZ-10 and (c) PZ-15	104
Figure 5.11 (a) Open-circuit voltage curves, (b) trend plots of open-circuit voltage (with statistical error-bars), (c) short-circuit current curves and (d) trend plots of short-circuit current (with statistical error-bars) of PZ-0, PZ-2.5, PZ-5, PZ-10 and PZ-15	106
Figure 5.12 (a) Charge produced by PZ-5 in shielded and unshielded mode and (b) effect of frequency (1 Hz, 2 Hz and 4 Hz) on open-circuit voltage of PZ-5	107
Figure 5.13 Stability of the PZ-5 device at 4 Hz frequency of impact force	107
Figure 5.14 (a) Voltage and current across load resistance of 50 k Ω to 50 M Ω , (b) power density curve of PZ-5	108
Figure 5.15 (a) Capacitor charging and discharging by PZ-5 device, illuminated red LED by charged 2.2 μ F capacitor (inset) and (b) circuit diagram for LED lighting	109
Figure 5.16 (a) working principle of PFM, ²³⁰ (b) amplitude PFM of PZ-0, (c) phase PFM of PZ-0, (d) amplitude PFM of PZ-5 (squared area representing nanocubes), (e) phase PFM of PZ-5 (squared area representing nanocubes), (f) amplitude and phase vs bias voltage plot of PZ-0 and (g) amplitude and phase vs bias voltage plot of PZ-5	109
Figure 5.17 (a)-(h) Steps of execution for application of PZ-5 as a touch sensor	111
Figure 5.18. (a) Schematic of PZ-5 as a temperature sensor by utilizing shape memory and piezoelectricity, (b) piezoelectric voltage output of PZ-5 as a function of temperature when heated from 40 $^{\circ}$ C to 60 $^{\circ}$ C during shape/strain recovery, (c) piezoelectric voltage of PZ-5 as a function of temperature, when cooled from 60 $^{\circ}$ C to 40 $^{\circ}$ C	113
Figure 6.1 FESEM morphology and cross-section of fibres inset of (a) PZ-0 (b) PZ-0.5	119
Figure 6.2 FTIR peaks of PZ-0, PZ-0.5, PZ-0.75 and PZ-1	120
Figure 6.3 XRD patterns of (a) ZT nanorod (m=0.04) and SMPU nanocomposite melt-spun filaments and individual XRD patterns of (b) PZ-0.5 (c) PZ-0.75 and (d) PZ-1 melt-spun filaments	122
Figure 6.4 DSC of (a) exothermic transitions in cooling cycle, (b) endothermic transitions in 2 nd heating cycle undergone by PZ-0, PZ-0.5, PZ-0.75 and PZ-1	123

Figure 6.5 (a) Open-circuit voltage, (b) bar graph (with error bars) of open-circuit voltage (c) short-circuit current, (d) bar graph (with error bars) of short-circuit current of PZ-0, PZ-0.5, PZ-0.75 and PZ-1, error bar representing standard deviation (S.D.).....	124
Figure 6.6 (a) Output charge in shielded and unshielded mode, (b) effect of frequency on open-circuit voltage of PZ-0.75	125
Figure 6.7 Stability of voltage output of PZ-0.75 (overall) and at different time intervals ..	126
Figure 6.8 (a) Capacitor charging (1 μ F, 2.2 μ F, 4.7 μ F) by voltage generation, (b) voltage and current at different load resistance, (c) power density of PZ-0.75	126
Figure 6.9 (a) Bar graphs representing strain fixity (%), (b) strain recovery (%), (c) fixed shape of PZ-0.75, (d) recovered shape of PZ-0.75	126
Figure 6.10 PFM Amplitude vs bias voltage plots of (a) PZ-0, (b) PZ-0.75, (c) random probe points in DART mode, (d) amplitude, (e) phase image of PZ-0.75	127
Figure 6.11 (a) Melt spinning process, (b) filament bobbins, (c) formation of shed by PZ-0.75 warp filaments, (d) insertion of PZ-0.75 weft and interlaced with warp yarns for formation of fabric, (e) original state of woven fabric prepared by PZ-0.75 filaments with 3M cloth tape in the selvedge and warp ends to hold the fabric structure tightly, (f) weft ends being stretched to 30% of its original length for its new fixed shape, (g) sensor prototype worn at wrist region	128
Figure 6.12 Open-circuit voltage generated by fabric in (a) original stage, (b) shape fixity stage	129
Figure 7.1 Strain fixity and recovery experiment of SMPU based electrospun nanofibres where sample is heated at temperature $> T_g$ [Image reproduced from ²¹¹].....	136
Figure 7.2 FESEM cross-sectional images of (a) PZR-1 along with magnified version of nanorods in the inset, (b) PZR-3 along with magnified version of nanorods in the inset, (c) PZR-5 along with magnified version of nanorods in the inset, (d) PZC-1 along with magnified version of nanocubes in the inset, (e) PZC-3 along with magnified version of nanocubes in the inset and (f) PZC-5 along with magnified version of nanocubes in the inset [Scale bar : 5 μ m and 500 nm (inset) for PZR-1,3,5; 10 μ m and 200 nm (inset) for PZC-1,3,5]	137
Figure 7.3 SEM images and size distribution profile of nanofibres in (a) PZR-1, (b) PZR-3, (c) PZR-5, (d) PZC-1, (e) PZC-3, (f) PZC-5	137
Figure 7.4 (a) Marked points in the control PZC/PZR-0 nanofibres used for measuring diameter, (b) size distribution of the nanofibres in the electrospun mat.....	138

Figure 7.5 Marked points in the nanofibres used for measuring diameter of (a) PZR-1, (b) PZR-3, (c) PZR-5, (d) PZC-1, (e) PZC-3, (f) PZC-5.....	138
Figure 7.6 TEM images of (a) PZR-1, (b) PZR-3, (c) PZR-5, (d) PZC-1, (e) PZC-3, and (f) PZC-5.....	139
Figure 7.7 DSC plots of (a) cooling cycle of PZR-0, PZR-1, PZR-3 and PZR-5, (b) 2 nd heating cycle plots of PZR-0, PZR-1, PZR-3 and PZR-5, (c) cooling cycle of PZC-0, PZC-1, PZC-3 and PZC-5 and (d) 2 nd heating cycle plots of PZC-0, PZC-1, PZC-3 and PZC-5.....	140
Figure 7.8 FTIR-ATR plots of (a) SMPU nanofibres with ZT nanorods, (b) SMPU nanofibres with ZT nanocubes.....	141
Figure 7.9 XRD plots of (a) ZT rods incorporated SMPU nanofibres, (b) ZT nanocubes incorporated SMPU nanofibres.....	142
Figure 7.10 Open-circuit voltage plots of (a) PZR-1, (b) PZR-3, (c) PZR-5, (d) PZC-1, (e) PZC-3, (f) PZC-5	143
Figure 7.11 Short-circuit current plots of (a) PZR-1, (b) PZR-3, (c) PZR-5, (d) PZC-1, (e) PZC-3, (f) PZC-5	144
Figure 7.12 (a) Mechanism of piezoelectricity, (b) orientation of high aspect ratio nanorods and distribution of nanocubes in electrospun nanofibres.....	145
Figure 7.13 (a) Mean open-circuit voltage bar graphs and (b) mean short-circuit bar graphs of PZR-1, PZR-3, PZR-5, PZC-1, PZC-3, PZC-5.....	145
Figure 7.14 (a) Open-circuit voltage, (b) short-circuit current and (c) charge of PZC-0/PZR-0.....	146
Figure 7.15. Effect of frequency (1 Hz, 2 Hz and 4 Hz) on open-circuit voltage of (a) PZR-1 and (b) PZC-1	146
Figure 7.16 Stability of open-circuit voltage plots of (a) PZR-1 and (b) PZC-1 (and voltage across 3 time intervals in the inset).....	147
Figure 7.17 Capacitor charging and discharging behaviour of (a) PZR-1 and (b) PZC-1 by 1 μ F, 2.2 μ F and 4.7 μ F capacitor.....	147
Figure 7.18 Practical demonstration of device utility by LED lighting of (a) PZR-1 and (b) PZC-1; powering of calculator by (c) PZR-1 and (d) PZC-1	148
Figure 7.19 (a) Voltage and current across load resistance and (b) Power density of PZR-1	148
Figure 7.20 (a) Voltage and current across load resistance and (b) power density of PZC-1	149

Figure 7.21 (a) Digital photograph of the electrospun piezoelectric device and (b) flexible nature of the device	149
Figure 7.22 Charge measured in shielded and unshielded mode from (a) PZR-1, (b) PZC-1	150
Figure 7.23 (a) Amplitude and Phase vs bias voltage of PZR-1, PFM Amplitude/Phase images (inset) and (b) amplitude and Phase vs bias voltage of PZC-1, PFM Amplitude/Phase images (inset).....	151
Figure 7.24 (a) Fixed and recovered shape of PZR-1, (b) fixed and recovered shape of PZC-1 (c) Strain fixity and recovery ratios of PZC/PZR-0, PZR-1, PZR-3, PZR-5, PZC-1, PZC-3 and PZC-5 at the end of 3 rd cycle of loading and unloading	151
Figure 7.25 (a) Original shape and fixed shape of multifunctional sensor PZC/R-X, (b) different flex condition of finger in ‘static’. ‘slightly bent’ and ‘fully bent’ conditions, (c) Prototype of the sensor fixed on finger, (d)-(f) output voltage waveforms of PZR-1 due to flex movements recorded on oscilloscope screen, (g) typical voltage waveform plot of PZR-1, (h)-(j) output voltage waveforms of PZC-1 due to flex movements recorded on oscilloscope screen, (k) typical voltage waveform plot of PZC-1.....	152
Figure 7.26 (a)-(c) Voltage waveform generated by PZR-1 during respiratory movement, (d) –(f) voltage waveform generated by PZC-1 during respiratory movement, (g) typical voltage waveform of PZR-1 during inhalation and exhalation, (h) typical voltage waveform of PZC-1 during inhalation and exhalation, (i) prototype of device fixed on N95 mask worn by user	154

List of Tables

Table 2.1 Comparison between physical properties of PZT and PVDF.....	16
Table 3.1 Average readings of tenacity (gf/den), strain at maximum load (%) and modulus (gf/den) values	51
Table 4.1.1 Crystallite sizes of intense peaks present in 0.15 M and 0.25 M NaOH concentration.....	61
Table 6.1 List of wavenumbers and respective characteristic bands of PZ-0, PZ-0.5, PZ-0.75 and PZ-1	121
Table 7.1 Wavenumbers (in cm^{-1}) of PZR-0, PZC-0, PZR-1, PZR-3, PZR-5, PZC-1, PZC-3 and PZC-5	142

LIST OF ABBREVIATIONS

PZT	Lead Zirconate Titanate
BaTiO₃	Barium Titanate
KNN	Potassium Sodium Niobate
ZnSnO₃,ZT,ZS	Zinc Stannate
ZnO	Zinc Oxide
BiFeO₃	Bismuth Ferrite
SMA	Shape Memory Alloy
SMP	Shape Memory Polymer
PVDF	Polyvinylidene Fluoride
SMPU	Shape Memory Polyurethane
r-GO	Reduced Graphene Oxide
PU	Polyurethane
ATR-FTIR	Attenuated Total Reflection-Fourier Transform Infrared Spectroscopy
XRD	X-Ray Diffraction
UV-vis	Ultraviolet Visible
LED	Light Emitting Diode
CTS	Carpel Tunnel Syndrome
LN	Lithium Niobate
PVDF-TrFE	Polyvinylidene Difluoride-Trifluoroethylene
ZTO	Zinc Tin Oxide
FESEM	Field Emission Scanning Electron Microscope
PFM	Piezoresponse Force Microscopy
TGA	Thermogravimetric Analysis
TEM	Transmission Electron Microscopy
PE	Polarization-Electric Field
LCR	Inductance, Capacitance and Resistance
DSC	Differential Scanning Calorimetry
P_r	Remnant Polarization
Bi_{0.5}Na_{0.5}TiO₃	Sodium Bismuth Titanate
PT	Lead Titanate

BiMeO₃	Metal Oxides Of Bismuth
GaN	Galium Nitride
NaOH	Sodium Hydroxide
MoS₂	Molybdenum Sulphide
KNbO₃	Potassium Niobate
AgNbO₃	Silver Niobate
NaNbO₃	Sodium Niobate
LiTaO₃	Lithium Tantalate
eV	Electron Volts
MgO	Magnesium Oxide
BTO	Barium Titanate
PDMS	Polydimethyl Siloxane
MWCNT	Multiwalled Carbon Nanotube
TiO₂	Titanium Dioxide
PVC	Poly (Vinyl Chloride)
Nitinol	Nickel Titanium Alloy
T_g	Glass Transition Temperature
T_m	Melting Temperature
MWNT	Multiwalled Nanotubes
CNF	Carbon Nanofibre
SiC	Silicon Carbide
Ppy	Polypyrrole
POSS	Polyhedral Oligomeric Silsesquioxane
Ti-Ni-Cu	Titanium-Nickel-Copper
NdFeB	Neodymium-Iron-Boron
PLA	Polylactic Acid
PEA	Polyesteramide
AESO	Acrylate Epoxidized Soybean Oil
TMSPM	3-(Trimethoxysilyl) Propyl Methacrylate
PDA	Polydopamine
IR	Infrared
THDA	Trimethylhexamethylenediamine
PCL	Polycaprolactone

MDI	Methylene Diphenyl Diisocyanate
DUT	Device Under Test
MWS	Maxwell Wagner Sillars
AFM	Atomic Force Microscopy
DART	Dual AC Resonance Tracking Mode
DC	Direct Current
AC	Alternating Current
EDX	Energy Dispersive X-Ray
KBr	Potassium Bromide